C_2 product formation in the CO_2 electroreduction on boron-doped graphene anchored copper clusters

Balázs Barhács[a], Ewald Janssens[b], Tibor Höltzl[a,c,d]

Abstract

A possible remedy for the increasing CO_2 concentration in the atmosphere is capturing, and reducing it into valuable chemicals like methane, methanol, ethylene, ethanol, etc. However, the suitable catalyst for this process is still under extensive research. Small sized copper clusters have gained attention in the recent years due to their catalytic activity in CO_2 reduction reaction. Although C_{2+} products higher economic value, only the formation of C_1 products was investigated thoroughly. For the electrochemical reduction of CO_2, a supporting material is needed for small copper clusters. Graphene is a promising candidate, as is exhibits good mechanical and electrical properties however, the weak interaction of copper and graphene needs to be addressed. Our DFT computations also revealed, that small Cu clusters on boron-doped graphene support are promising catalysts for the electrochemical reduction of CO_2 towards both C_1 and C_2 products. We demonstrate the most promising reaction pathways towards various C_1 products, and ethanol or ethylene as C_2 products on both Cu_4 and Cu_7 clusters on a boron-doped graphene (BDG) support. We also demonstrate the size-tuneable reactivity of these materials: Cu_4 is considered a more reactive agent in general, but Cu_7 shows a higher selectivity towards C_2 products

a. Department of Inorganic and Analytical Chemistry, Budapest University of Technology and Economics, Szent Gellért tér 4, H-1111 Budapest, Hungary

b. Quantum Solid-State Physics, KU Leuven, Celestijnenlaan 200D, BE-3001 Leuven,Belgium

c. MTA-BME Computation Driven Research Group, Budapest University of Technology and Economics, Szent Gellért tér 4, H-1111 Budapest, Hungary

d. Furukawa Electric Institute of Technology, Nanomaterials Science Group, Késmárk utca 28/A, H-1158 Budapest, Hungary

1. Introduction

The continuously increasing atmospheric CO_2 concentration due to the combustion of an enormous amount of fossil fuels leads to severe problems of the global warming and the decreased hydrosphere pH. (1; 2; 3; 4; 5; 6; 7; 8) Capturing CO_2 and reducing it to useful chemicals like methane, methanol, ethylene, ethanol, etc., is a promising solution to mitigate this problem (8; 9; 10). Although the CO_2 hydrogenation is thermodynamically feasible, in practice, it is hindered by high kinetic barriers, thus a proper catalyst is required for this process. (11)

It is well known since the seminal works of Hori et al. that the electrolysis of bicarbonate solution using copper electrode produces not only hydrogen, but also methane, ethylene, and higher organic compounds. (12). Decreasing the catalyst size to the nano- and - scale was shown to be a fruitful strategy to increase the catalytic activity, thus along the Cu surfaces (13; 14; 15; 16; 17; 18; 19; 20; 21), nanoparticles (22; 23; 24), and small Cu clusters were also investigated as active catalysts for CO_2RR (25; 26; 27; 28; 29; 30).

Metal clusters are particularly promising due to their very high atom-efficiency. Liu et al. studied CO_2RR on small sized, four atom copper clusters deposited on an alumina surface using both experimental techniques and theoretical methods. (27) Cu_4 exhibited an excellent catalytic activity, with methanol as the main product, while due to the relatively low activation barriers methane is also formed. Later they investigated the cluster size effect in the reaction towards methanol (30) and found, that the size-dependence of reactivity is non-monotonous: Cu_4/Al_2O_3 is the most reactive followed by Cu_{20} and Cu_3. Tao et al. investigated the cluster size effect on TiO_2 (110) supported clusters and also found, that Cu_4 exhibits the highest activity for converting CO_2 to methanol. (29) Yang et al. studied Fe_2O_3 supported Cu_4 clusters in the same reaction and concluded that Cu_4 facilitates the H_2 dissociation and spill-over, leading to the reduction of the oxide surface as Fe^{2+}-Cu_4, what promotes CO_2 activation. (31)

Depending on the energy source the CO_2 reduction reaction (CO_2RR) can be activated thermally (32), photocatalytically (9; 33), and electrocatalytically (12; 34), the latter being particularly promising due to its efficiency. The conductive support for electrocatalysts is highly important. A promising candidate for the support material is graphene, not only because of its advantageous mechanical and electronic properties (35; 36) but it can also synergistically enhance the activity of the supported catalyst (37; 38; 39; 40; 41).

Curtiss et al. investigated four atom transition metal clusters and found that they are promising candidates for the CO_2 electrochemical reduction. The overpotentials for producing CH_4 were in the following order: $Co_4 < Fe_4 < Ni_4 < Cu_4 < Pt_4$. They also investigated the effect of a defective graphene support in the case of Cu_4 and calculated lower limiting potentials for CH_4 production compared to a Cu (111) surface (26). Xu et al. synthesized a carbon-supported copper catalyst using an amalgamated Cu-Li method, and it was shown, that the copper aggregation state has a significant effect on the faradaic efficiency of ethanol. They observed high activity for small clusters, but their aggregation to larger Cu and CuO clusters decreased the faradaic efficiency. DFT calculations clearly showed that small clusters play an important role in the catalytic activity. (42)

In comparison with C_1 species, C_{2+} species have higher economic value due to their wider industrial usability (43), thus nowadays the product selectivity is being studied extensively on various catalysts, including metal surfaces and nanoparticles. While recent experimental results showed promising formation of ethanol on small copper clusters (42) and the efficient conversion of syngas to C_2 products on MoS_2 anchored Cu_4 clusters was demonstrated using theoretical methods, (25) the detailed understanding of the C_2 product formation mechanism on metal clusters is still not available. Here we investigate copper cluster anchoring to boron doped graphene using nanoflake model and its efficiency for the CO_2 reduction towards both C_1 and C_2 products.

2. Computational details

All calculations were carried out using the Q-Chem 5.2 and 5.3 program packages. We used the PBE density functional (44) with an additional empirical dispersion correction (Grimme DFT-D2) (45), and the def2-TZVP basis set (46). The accuracy of the selected method was confirmed by CCSD(T)/def2-TZVPPD benchmark computations on small model systems (see the Supporting Information for the details).

The reaction intermediates were optimized, and the solvation free energies were computed in water solvent using the SMD implicit solvent model (47). The reaction free energies were calculated using the Computational Hydrogen Electrode (CHE) model (19), what was successfully applied to explore the CO_2RR reaction mechanism on metal clusters (48; 26). CHE assumes that the proton in each reaction step comes from a H^+ transport chain in the aqueous electrolyte and is reduced simultaneously by the electrons from the supporting electrode. It must be noted that the accurate determination of the barrier of this reaction is a highly complex task,

and it depends on the operational conditions (particularly the electric potential, the chemical composition of the electrolyte and its concentration) thus its determination is beyond the scope of our paper. Recent grand-canonical Density Functional Theory computations showed that this barrier equals to about 0 to 50 kJ/mol in the case of for CO_2 hydrogenation (49; 14).

We interpret the non-covalent interaction of the clusters and the Boron Doped Graphene (BDG) nanoflake based on the Complementary Occupied-Virtual Pairs (COVP), computed using Energy Decomposition Analysis based on Absolute Localized Molecular Orbitals (ALMO-EDA) (50). Natural Atomic charges were obtained from Natural Bond Orbital (NBO) analysis (51). We also calculated the Nucleus-Independent Chemical Shift (NICS) values (52) for the BDG model compared to benzene, as a probe of aromaticity.

3. Results

Anchoring atoms and doping patterns

It is well known that the interaction between graphene and copper is relatively weak (53; 54) and chemical modification is necessary for efficient anchoring. Thus, for the graphene support three important model features must be selected: the dopant element, the dopant pattern, and the model geometry.

Here we selected boron as anchoring atom due to its high binding affinity to copper clusters (see the Supporting Information for the details) and as boron doped graphene allows the single copper atoms aggregation to clusters (55). Pure graphene also has a significant electrocatalytic effect, what is increased by doping with almost any other element (41), with boron doping among the few exceptions (56). This suggests that the anchored metal cluster and its interaction with the support is responsible for the catalytic activity. In line, Joshi et al. investigated boron-doped graphene as a support for IrO_2 nanoparticle catalysts for oxygen evolution reaction and found that not only did the boron-doping increase the stability of IrO_2 nanoparticle-graphene complex, but also lead to stronger binding of the reaction intermediates to the nanoparticle, resulting in increased reactivity (39). It is also interesting to note that boron doping of copper leads to efficient C_2 hydrocarbon productions in CO_2RR (57). For the dopant pattern we selected a similar structure to the well-known graphitic carbon-nitride, what was shown in reference for boron (47). Here three-dopant atoms surround a vacancy, such that each atom bears its formal valency. Finally, we selected finite flake models, which was motivated by the experimentally limited crystallinity of the doped graphene and also from the theory side by the applicability of the well-established quantum chemical wavefunction analysis tools. A

sufficiently large model system is necessary, as in finite polycyclic aromatic hydrocarbons (PAHs), copper clusters prefer to bind to the PAH edges (58).

Our model system is based on a small graphene nanoflake, where the central carbon atom is removed, and the vacancy is surrounded by boron atoms. The initial nanoflake is a non-Kekulé molecule which has a doublet ground state. If we remove the central carbon atom from the PAH and substitute the surrounding three carbon atoms with boron (Figure 1), that results in a molecule with the chemical formula of $C_{33}H_{15}B_3$, which has a singlet ground state.

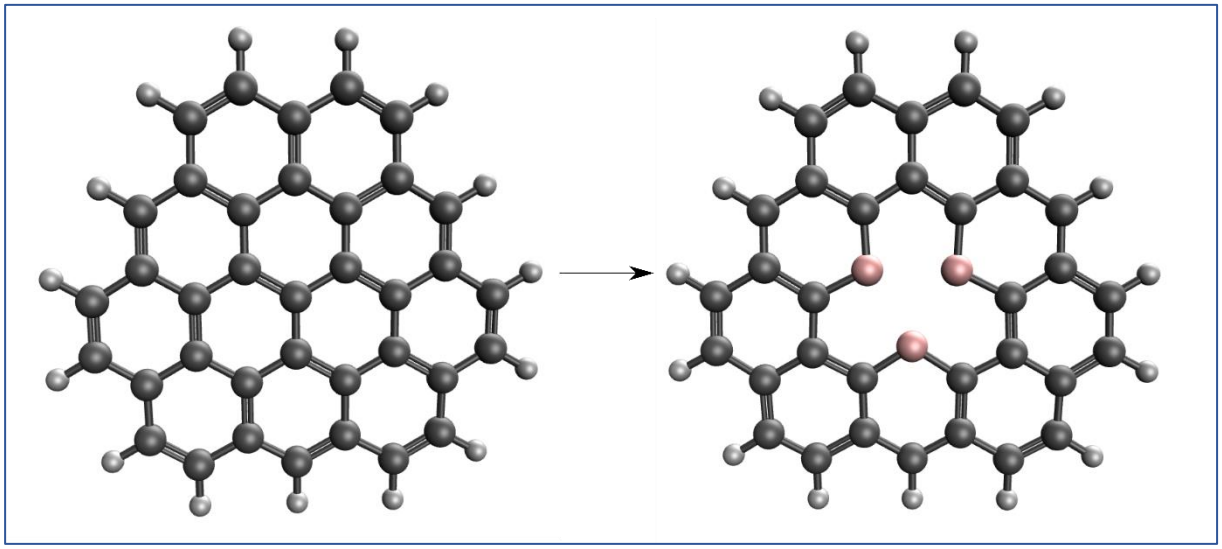

Figure 1.Construction of BDG nanoflake model

The highly negative NICS(1) ((when the ghost atom is placed 1Å above the centre of the ring, see the Supporting Information for the justification of this choice) values of -8.9 ppm of our nanoflake model molecule compared to -9.8 ppm of that of the benzene shows that our model system is aromatic, what suggests and enhanced stability of this particular doping pattern. The Wiberg bond indices between the carbon atoms are in the range of 1.2-1.3, which are between those of the ideal single and double C-C bonds and are close to the ~1.4 C-C Wiberg bond indices of the aromatic benzene. The B-C bonds had a value of ~1.07, and the B-B ~0.4. Investigating the occupied molecular orbitals of this system, we found, that both the lowest energy σ and the lowest energy π orbitals are fully delocalized (Figure 2).

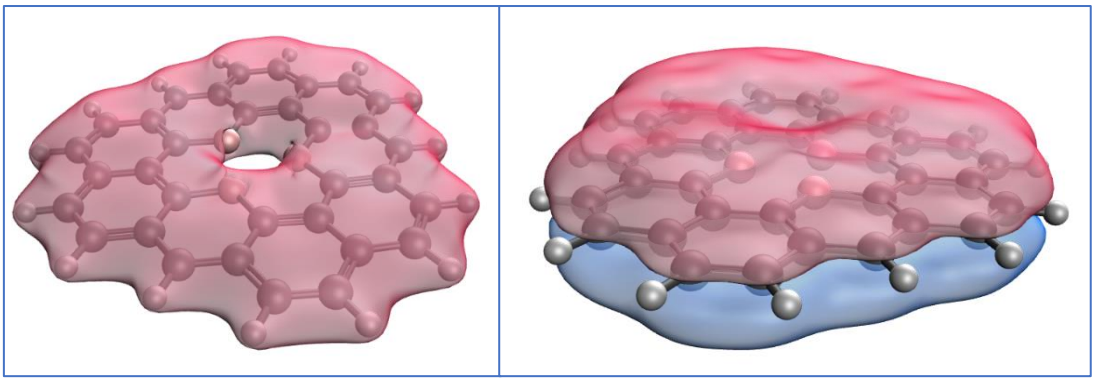

Figure 2. The delocalized σ and π orbitals of the BDG nanoflake

Copper cluster anchoring to BDG nanoflakes.

The optimized geometrical structures of the free, gas phase and the BDG nanoflake anchored Cu_n (n=3-8) clusters and the natural charges of each Cu atom are depicted in Figure 3. The interaction energies between the different sized copper clusters and the BDG nanoflake and the natural charges are available in Table 1.

Table 1. The cluster-BDG interaction energies and the natural charges of BDG bound clusters

$C_{33}H_{15}B_3Cu_n$	Interaction energy (kJ/mol)	Cluster natural charge
1	-326	0.731
2	-389	1.48
3	-538	2.08
4	-507	2.13
5	-577	2.11
6	-568	2.06
7 (a)	-527	2.00
7 (b)	-557	2.08
8 (a)	-490	1.98
8 (b)	-552	2.03

The cluster-BDG interaction energy increases monotonically until n=3, while weaker, non-monotonic size-dependence is observed for larger clusters. (Table 2). It is also well visible that the surface anchored Cu_n clusters exhibit partially positive charges, which saturate at approximately +2 at n=3. The excess positive charges reside mainly on the boron bound copper atoms (Figure 3). This and the clear correlation between the increase of cluster natural charges

clearly show that the boron-bound copper atoms of the cluster are responsible for the interaction.

We also found that the clusters coordinate to three boron atoms of the surface. If we compare the gas-phase geometries to the clusters on BDG, the first noticeable difference is that while the gas-phase Cu_4 is planar, the cluster on BDG exhibits an interesting, almost perfect tetrahedral shape. In case of Cu_5 and Cu_6, the most stable structure in gas phase is also planar, but the BDG anchoring leads to three-dimensional cluster shapes.

Two different $BDGCu_7$ and Cu_8 isomers are located. The most stable BDG bound structures (structure "b") are also polyhedrons, but their most stable geometries differ from those of the gas phase clusters. The most stable gas-phase structure of Cu_7 is a hexagonal bipyramid, and a similar structure exists also in the case of the BDG bound cluster, (Figure 3 – $BDGCu_7$(a)), however a more structure square pyramidal structure ($BDGCu_7$(b)) also exists. The shape of Cu_8 also differs from the gas phase shape (Cu_8(a)) but is likely to form a Cu_7-like hexagonal bipyramid with an additional tetrahedron, so that the subsequent Cu atom can also bind to the surface. (Cu_8(b)).

As we will see later in our article, not only the more stable structure Cu_7(b), but also Cu_7(a) occurs in several reaction intermediates, which shows that the cluster geometry can dynamically change during the CO_2RR.

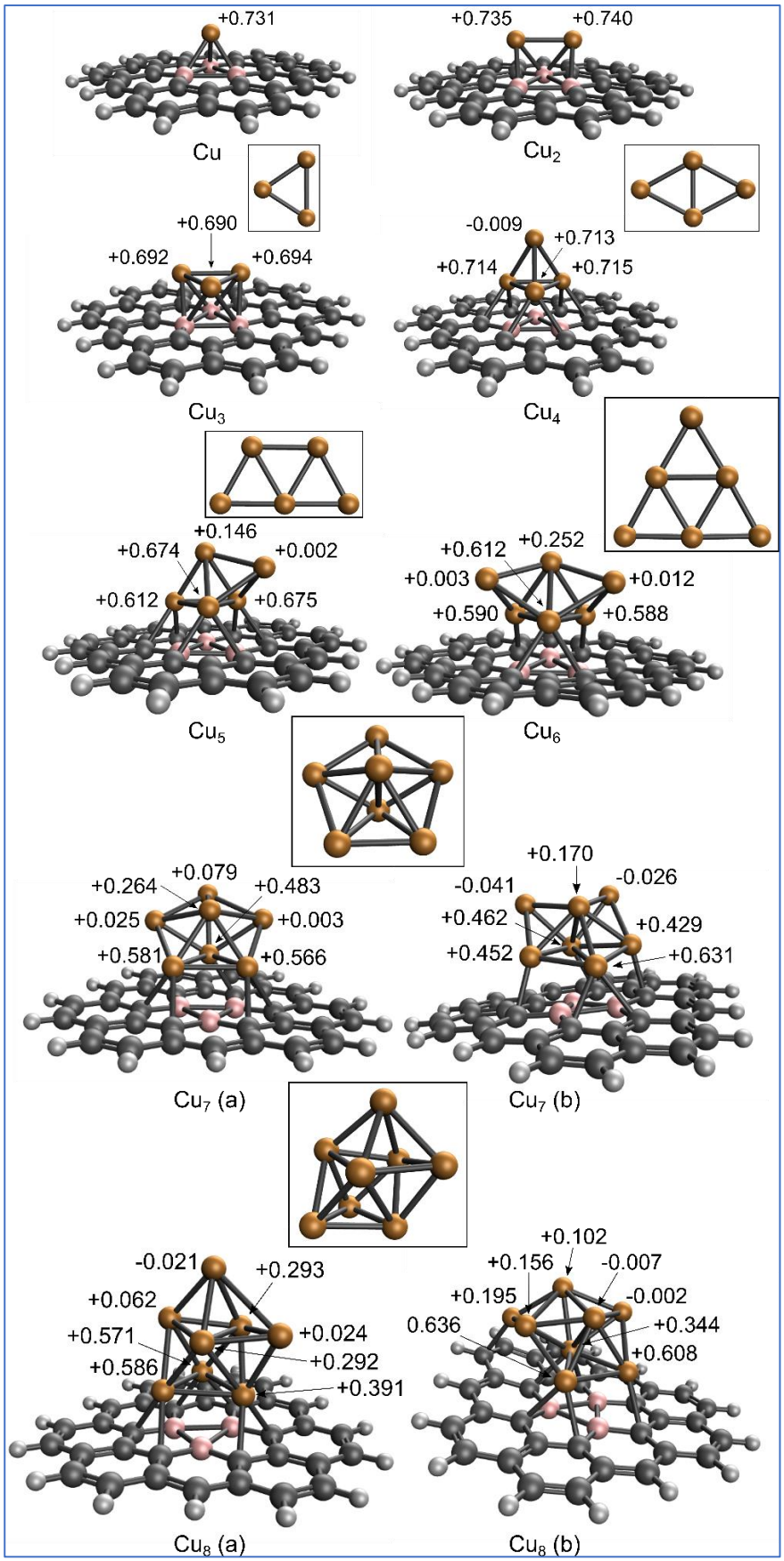

Figure 3. The optimized structures of gas phase and BDG supported clusters. The natural charges of Cu atoms are also shown in the case of BDG supported clusters.

The almost perfect, tetrahedral shape of Cu_4 cluster on BDG is in line with the electron donation from the Cu cluster to the surface: the cluster therefore obtains an approximately +2 natural charge. This can be interpreted with the Phenomenological Shell Model (PSM) (59): the $4s^1$ electrons of Cu atoms are itinerant, which for the neutral Cu_4 cluster leads to the $1S^2\ 1P^2$ electron configuration (we note the cluster orbitals from the PSM with capital letters). However, there are only two itinerant electrons in the formally di-cationic Cu_4 cluster, which corresponds to $1S^2$ closed electronic structure, which is a closed electronic structure and implies and extended stability.

Electronic structure analysis of the anchoring

We investigated the most relevant COVP pairs for all BDG bound clusters ($BDGCu_n$) mentioned before. All of the mentioned ALMOs are noted with capital letters according to the PSM (S,P,D) if they belong to the metal cluster, and with Greek letters commonly used for molecular orbitals, if the ALMO belongs to the BDG nanoflake. The detailed results for n=4 are presented here, while the analogous results for other cluster sizes are available in the Supporting Information. According to the PSM, the gas phase Cu_4 cluster has four itinerant electrons, which corresponds to $1S^21P^2$ electronic structure.

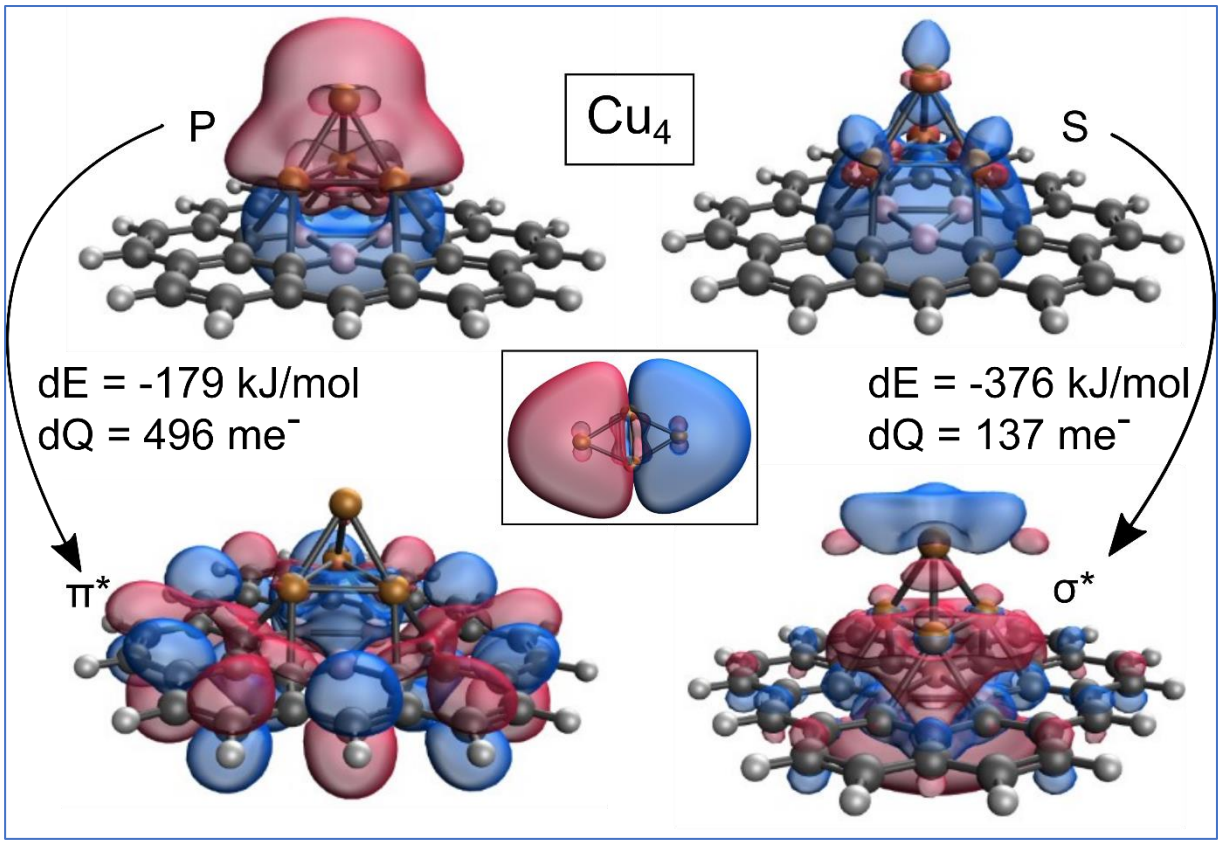

Figure 4. The most relevant COVP pairs of the $BDGCu_4$ system

The COVP analysis shows that during the anchoring the P orbital of the cluster donates electron to the BDG π* orbital. This process involves the transfer of approx. half an electron charge from the cluster to the BDG. The second relevant donor is an S orbital of the cluster, what donates to a σ* orbital of the BDG nanoflake. The charge transfer is much smaller in this case in this case, but the energy contribution is relatively high.

For n>2 the main charge transfer is due to the electron donation from the clusters' P orbitals to the π* orbitals of the BDG nanoflake. This π* orbital consists of both the p atomic orbitals of carbon and boron atoms however, it contains the p orbitals of the three boron atoms with higher coefficients (so that the ALMO seems to have a delocalized domain in the centre of the ring). This ALMO corresponds formally to the LUMO of the individual BDG nanoflake (Figure 4). Likewise, the HOMO of the individual gas phase clusters is a P orbital in all cases. The second relevant donor ALMO is a cluster S orbital, and the acceptor is a σ* orbital of the boron atoms. It must be noted that D shell orbital also participates in the chemical bonding.

Overall, we can conclude that the interaction energy of the copper clusters and the BDG nanoflake mostly due to the the significant charge transfer between the two fragments. The

cluster donates electrons to the BDG nanoflake. In this interaction, the boron atoms have a significant role: they have the highest eigenvalues in the acceptor ALMOs (both π* and σ*).

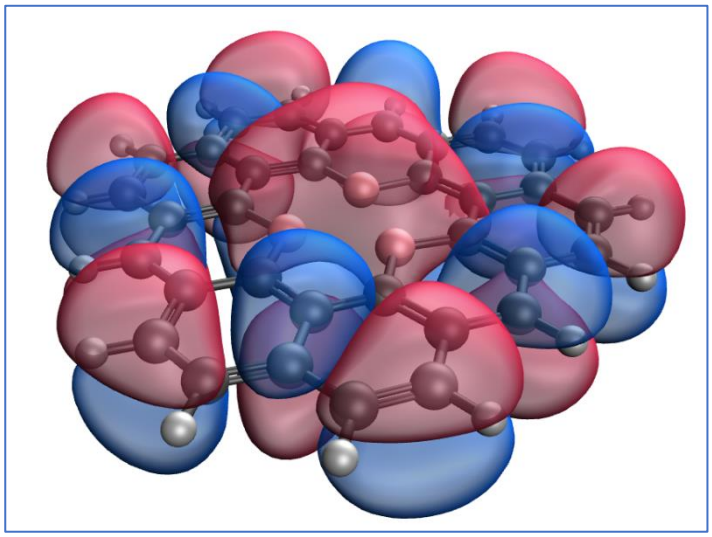

Figure 5. The LUMO of the BDG nanoflake

Descriptors for C_2 formation

It was shown recently that the potential-determining (and thus the rate-determining) step of the CO_2RR reaction towards C_2 products is the C-C coupling through the reductive dimerization of two CO molecules (13; 20; 21; 60):

$$* CO + * CO + \frac{1}{2} H_2 = * OCCOH,$$

where asterisks denote catalyst surface bound species.

Thus, according to the results of Huang et.al. (22), the reaction energy towards *OCCOH can be used as reactivity descriptor to estimate the feasibility of CO_2RR toward C_2 products with various catalysis:

$$\Delta E_{OCCOH} = E(* OCCOH) - 2 \cdot E(* CO) - \frac{1}{2} \cdot E(H_2)$$

The lower this descriptor is, the higher the CO_2RR rate towards C_2 products.

We computed the reaction energy of this C-C coupling step on all sites of the cluster for $BDGCu_n$, (n = 3-7), and the reaction energies on the most reactive site of each cluster are listed in Table 2.

Table 2. The reaction energies of the C-C coupling step on different sized BDG bound copper clusters

$BDGCu_n$	ΔE_{OCCOH} (kJ/mol)
Cu_4	112
Cu_5	29
Cu_6	36
Cu_7	28

This C-C coupling step is always endothermic and is expected to be least favoured for n=4, while for larger clusters weak size-dependence is observed. Thus, for detailed comparison of the reactivities, we computed the whole reaction paths towards C_1 or C_2 products for both the Cu_4 and Cu_7 clusters.

Reactions towards C_1 products

We first located the most stable electrochemical binding site of CO_2, then systematically investigated the possible reduction pathways. The most feasible reaction paths are depicted in the figures below, while the higher energy pathways are available in the Supporting Information.

a)

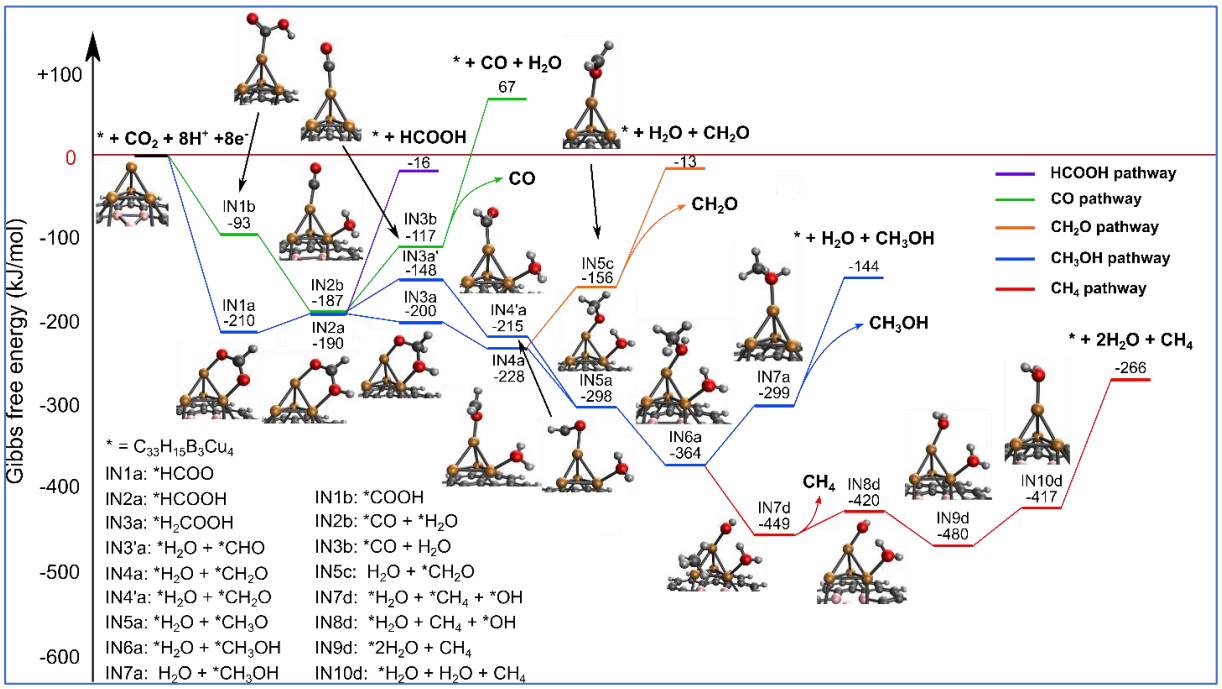

b)

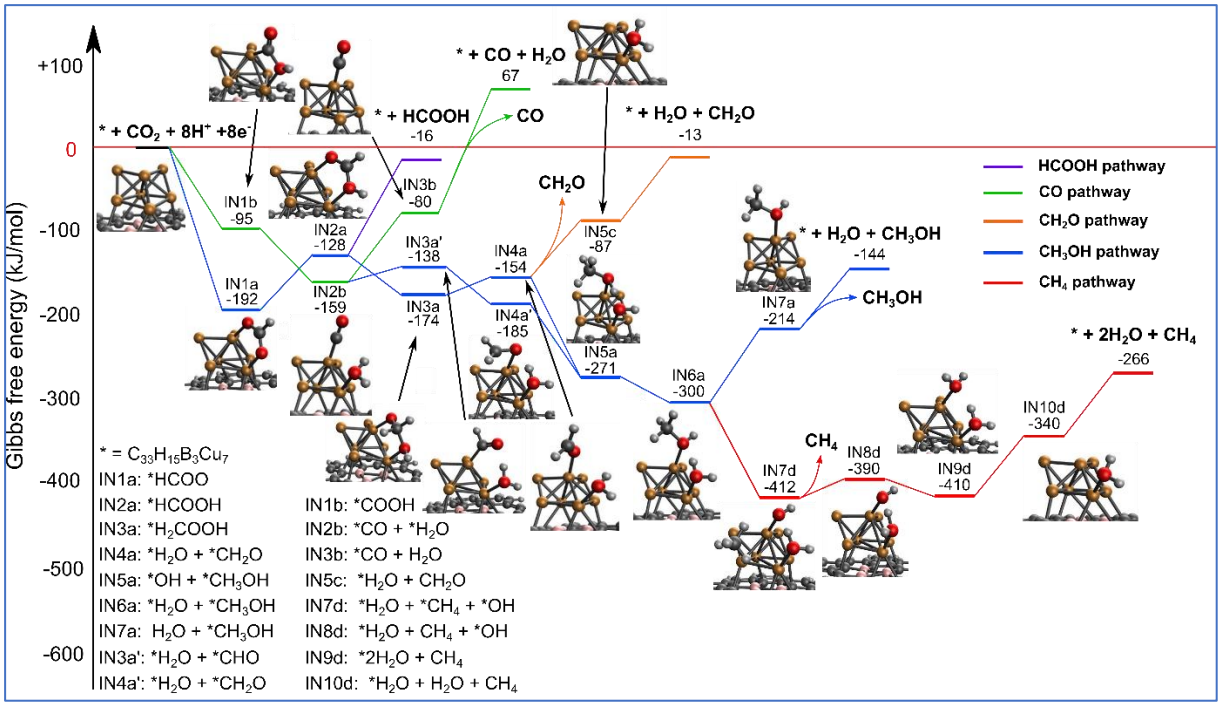

Figure 6. C_1 reaction pathway in an aqueous solution at 298K, 1 atm using different size cluster catalysts a) $BDGCu_4$ b) $BDGCu_7$

Figure 6 shows the reaction paths towards C_1 products using $BDGCu_4$ and $BDGCu_7$ catalysts, respectively. It is well visible that the different reaction paths diverge already at the first step, when CO_2 is electrochemically adsorbed and reduced to either carboxyl (*COOH, green line) or formate group (*HCOO, blue line). The further reduction of *COOH leads to adsorbed *CO, whose desorption from the cluster is thermodynamically unfavoured. The further hydrogenation of *CO to *CHO (blue line, higher in free energy) leads to $*CH_2O$ (formaldehyde) and subsequently to $*CH_3O$. It is interesting to note that the $*CH_3O$ intermediate can be also reached by the further consecutive reduction of *HCOO through formic acid (*HCOOH) and $*H_2COOH$. This is in line with the previously found reaction paths on deposited Cu_4 clusters (27; 30). The C-O bond breaks during the further reduction of $*H_2COOH$ and formaldehyde ($*CH_2O$) is formed. Desorption of formaldehyde or formic acid is thermodynamically unfavoured. Thus, the further hydrogenation of $*CH_3O$ leads to methanol. The desorption of methanol is also an endergonic step. The further reduction of the adsorbed methanol $*CH_3OH$ leads to C-O bond breaking, and methane is formed. Methane eliminates easily from the cluster.

The green and blue reaction paths are analogous to the widely accepted ones for methanol formation on various copper surfaces (17; 18) and nanoparticles (23). Interesting difference between $BDGCu_4$ and $BDGCu_7$, is that the diverging blue reaction paths cross only in the latter case. Consequently, the reactivity of $BDGCu_4$ differ more from that of Cu surfaces, thus this cluster can open new reaction paths. Also, the different relative free-energies of the intermediates imply that the methanol formation is somewhat more favoured in the case of $BDGCu_4$ than on $BDGCu_7$, which opens the possibility to tune the product composition by the cluster size.

Also, it was shown for Cu surfaces, that methane forms not from the hydrogenation of $*CH_3O$ (or $*CH_3OH$), but through a different pathway, where from *CO *COH if formed instead of *CHO, and after a C-O bond breaking, water and $*CH_x$ (x=0,1,2,3) species are formed resulting in methane. We computed the formation of *COH however, it is highly endergonic (See Supporting Information for details). This suggests that on small metal clusters this pathway is thermodynamically blocked.

The simplified depiction of the C_1 reaction pathways on the BDG supported clusters is shown in Scheme 1 with green background. Our computations show that on BDG supported

small Cu clusters, the main C_1 products are methanol and methane with higher ratio of methanol in the case of $BDGCu_4$ than $BDGCu_7$.

Reactions towards C_2 products

To the best of our knowledge, the electroreduction reaction pathways have not been reported yet for C_2 products on metal clusters, thus we systematically investigated the analogous reaction path to those proposed by Kortlever et.al. (34) and Xiao et. al. (21) for Cu towards ethylene and ethanol.

a)

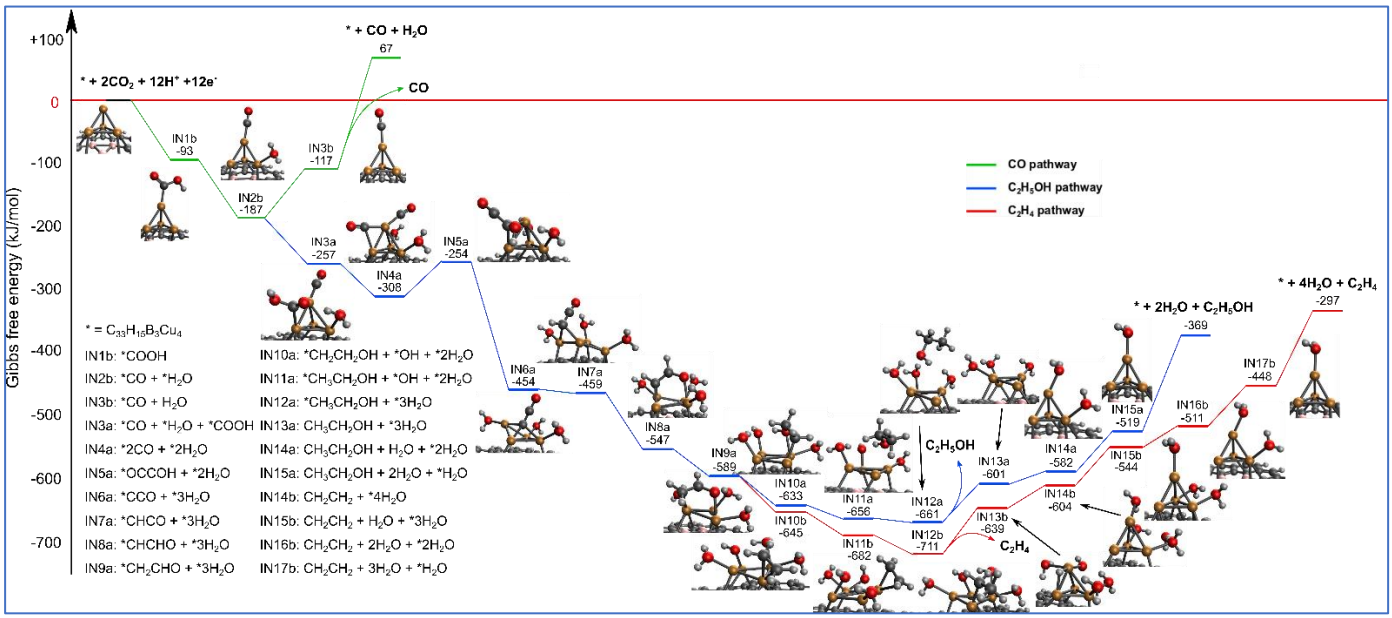

b)

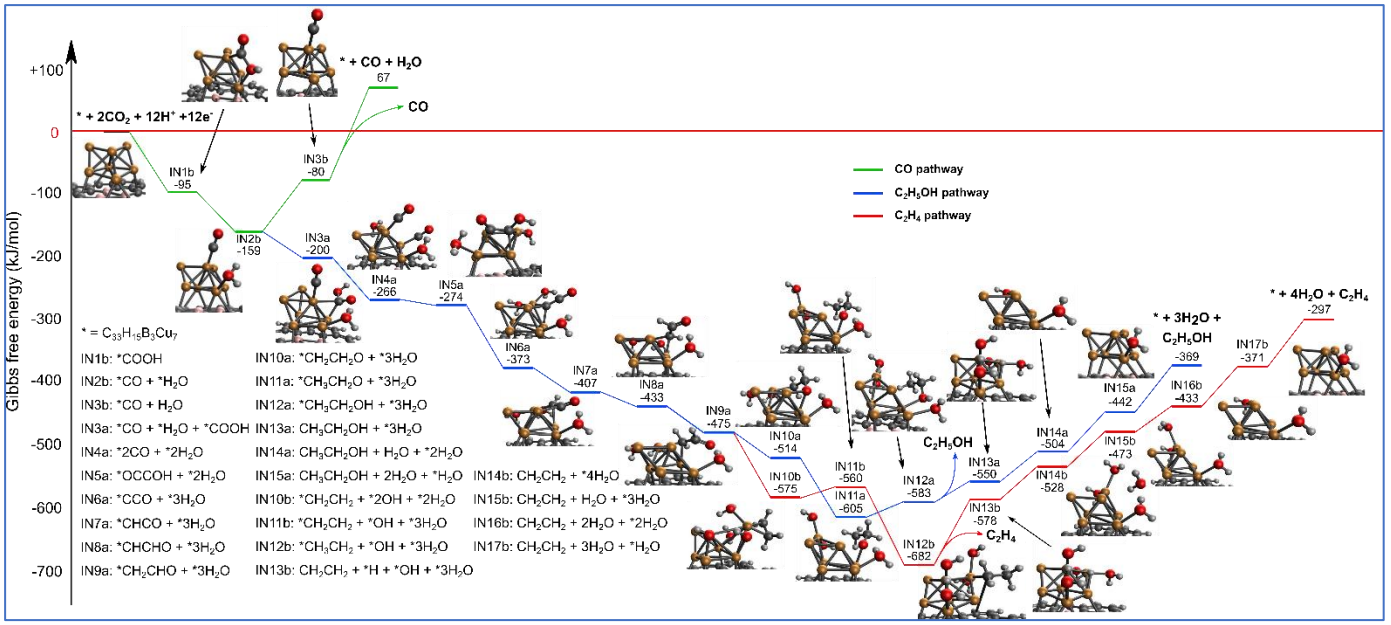

Figure 7. C_2 reaction pathway in an aqueous solution at 298K, 1atm using different size cluster catalysts a) $BDGCu_4$ b) $BDGCu_7$

The most favoured reaction paths are depicted in Figure 7. As we described above, the important step of the formation of C_2 products is the C-C coupling through the reductive dimerization of two catalyst surface bound *CO molecules, thus the reaction starts with subsequent partial reductions of two CO_2 molecules, what is followed by the reductive dimerization and the formation of *OCCOH.

It is interesting that in the gas phase reactions, this is always an endothermic step (see Supporting information for the gas phase reaction pathways): there is a +71 kJ/mol reaction energy for $BDGCu_4$ and only +39 kJ/mol for Cu_7 at this step. This is a smaller value for $BDGCu_4$ and larger for $BDGCu_7$ than the values computed as a reactivity descriptor before. On the other hand, the solvation makes this step thermodynamically feasible in the case of $BDGCu_7$, thus the solvent changes even the qualitative reactivity.

The fact that the C-C coupling is more likely to occur on the larger cluster may have also steric reasons due to the relatively crowded arrangement of the several reactants on the Cu_4 cluster.

Following the further hydrogenation of *OCCOH and C-O bond breaking, water dissociates and *CCO forms. Here, the tetrahedral shape of Cu_4 on BDG opens, and it recovers only after the desorption of product molecules. *CCO is then further hydrogenated to *CHCO, *CHCHO, $*CH_2CHO$, where the reaction can continue in two different pathways. We denote the formation of ethanol with blue, and ethylene with red line on the figure. For the blue path we found that from $*CH_2CHO$ intermediate the formation of $*CH_2CH_2O$ is more facile than that of the $*CH_3CHO$. Then on Cu_4 an adsorbed ethanol $*CH_3CH_2OH$ is formed directly from $*CH_3CH_2O$ by taking another hydrogen atom from an adsorbed H_2O molecule. On $BDGCu_7$, $*CH_3CH_2O$ is the most stable intermediate, and the $*CH_3CH_2OH$ formation is slightly endergonic. The dissociation of ethanol from both clusters is an endergonic process, indicated by the reaction free-energies of +60 kJ/mol for $BDGCu_4$ and +33 kJ/mol for $BDGCu_7$. This shows that the ethanol dissociation is more favoured on $BDGCu_7$ but it is thermodynamically not blocked even on $BDGCu_4$. At the red path, to form ethylene from $*CH_2CHO$, a C-O bond breaking is required after a $H^+ + e^-$ transfer. The desorption of ethylene from the cluster is always endergonic, thus the further reduction of the adsorbed ethylene to an ethyl group is more likely to occur. From here, the only possibility for ethylene production is the β-elimination step, as it was proposed by Xiao et. al (21) however, we found this step also endergonic (+72 kJ/mol for $BDGCu_4$ and +104 kJ/mol for $BDGCu_7$). An adsorbed hydrogen atom is also left on the cluster, that needs to form a water molecule with an adsorbed by-product *OH. The computed reaction pathways and reaction free energies clearly show, that BDG bound small Cu clusters can catalyze C_2 formation both towards ethylene and ethanol. A simplified summary of the C_2 reaction pathways is shown in Scheme 1 with blue background.

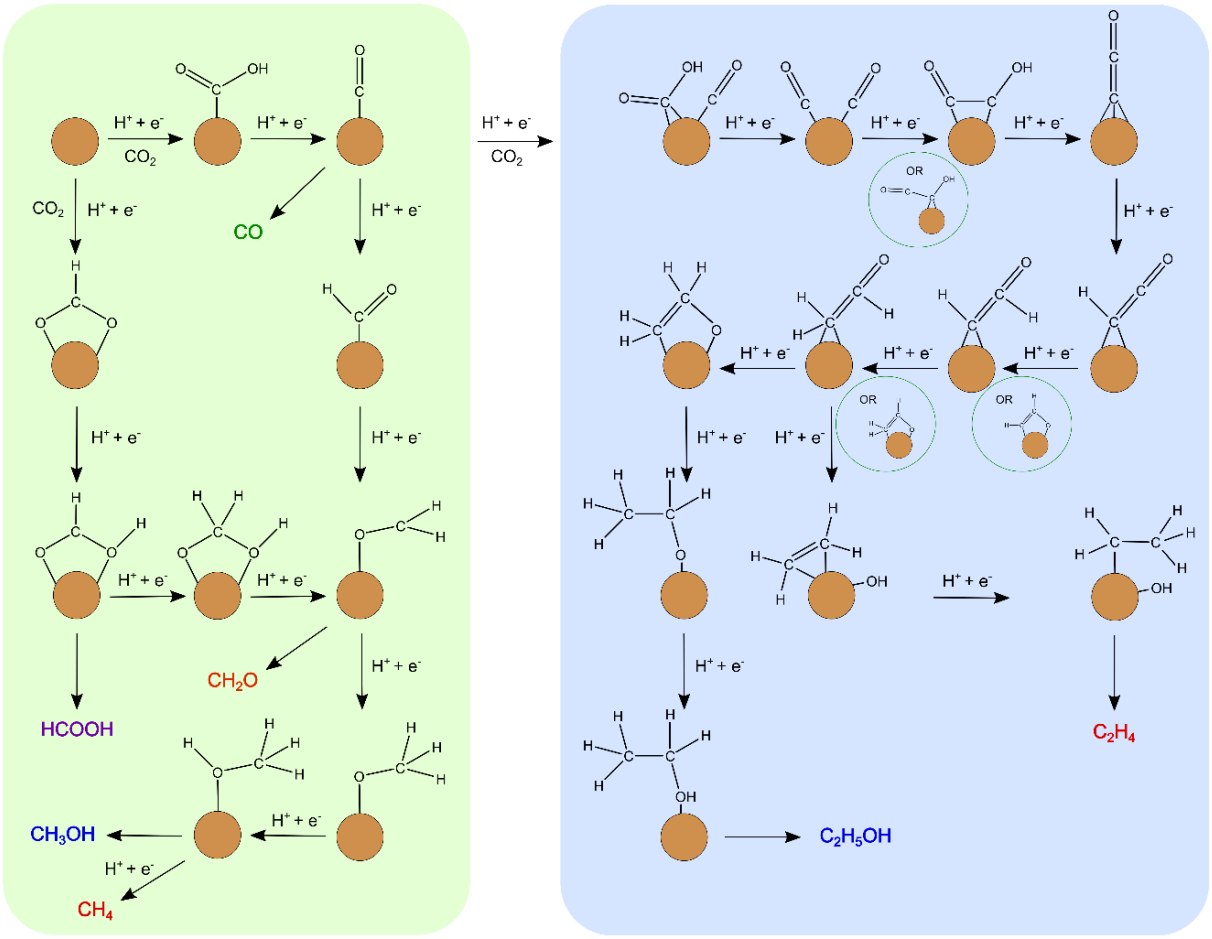

Scheme 1.

4. Conclusion

In summary, in this work we showed using a nanoflake model that boron doping is a promising method to immobilize small (n=3-8) Cu clusters on graphene and the resulting system has high catalytic activity in CO_2RR towards both C_1 and C_2 products. Our computations clearly showed that the large binding energies between the boron doped graphene nanoflake and the clusters are due to the charge transfer, as Cu clusters donate electrons mainly to the boron-atoms. In this complex, boron-doped graphene is the supporting electrode material and small Cu clusters exhibit catalytic activity in the electrochemical reduction of CO_2. The Gibbs-free energies along the possible reaction paths confirmed the catalytic activity of BDG supported Cu_4 and Cu_7 clusters for C_1 products. The size dependence is relatively weak but expected to allow the tuning of the methanol/methane product ratio. The investigation of the descriptors towards the C_2 products clearly showed that the BDG supported copper clusters are promising catalysts. The detailed reaction paths for the BDG supported Cu4 and Cu7 clusters confirmed this and also showed that BDGCu_7 shows an increased selectivity towards ethanol and ethylene.

Acknowledgments

This work is supported by the ÚNKP-20-1-I New National Excellence Program of The Ministry of Human Capacities. This work is supported by the KU Leuven–Budapest University of Technology and Economics joint research funding (CELSA/18/032). supported by the KU Leuven–Budapest University of Technology and Economics joint research funding (CELSA/18/032).

5. References

1. *Frontiers, Opportunities, and Challenges in Biochemical and Chemical Catalysis of CO2 Fixation.* **Appel, Aaron M., et al.** 8, 2013, Chemical Reviews, Vol. 113, pp. 6621-6658.

2. *Catalysis Research of Relevance to Carbon Management: Progress, Challenges, and Opportunities.* **Arakawa, Hironori, et al.** 4, 2001, Chemical Reviews, Vol. 101, pp. 953-996.

3. *Utilisation of CO2 as a chemical feedstock: opportunities and challenges.* **Aresta, Michele and Dibenedetto, Angela.** 28, 2007, Dalton Transactions, pp. 2975-2992.

4. *Catalysis for the valorization of exhaust carbon: from CO2 to chemicals, materials, and fuels. technological use of CO2.* **Aresta, Michele, Dibenedetto, Angela and Angelini, Antonella.** 3, 2014, Chemical Reviews, Vol. 114, pp. 1709-1742.

5. *Prospects for conversion of solar energy into chemical fuels: the concept of a solar fuels industry.* **Harriman, Anthony.** 1996, 2013, Philosophical Transactions of the Royal Society A, Vol. 371, pp. 20110415-20110415.

6. *Powering the planet: Chemical challenges in solar energy utilization.* **Lewis, Nathan S. and Nocera, Daniel G.** 43, 2006, Proceedings of the National Academy of Sciences of the United States of America, Vol. 103, pp. 15729-15735.

7. *A global review of energy consumption, CO2 emissions and policy in the residential sector (with an overview of the top ten CO2 emitting countries).* **Nejat, Payam, et al.** 2015, Renewable & Sustainable Energy Reviews, Vol. 43, pp. 843-862.

8. *CO2 Hydrogenation to Formate and Methanol as an Alternative to Photo- and Electrochemical CO2 Reduction.* **Wang, Wan Hui, et al.** 23, 2015, Chemical Reviews, Vol. 115, pp. 12936-12973.

9. *Status and perspectives of CO2 conversion into fuels and chemicals by catalytic, photocatalytic and electrocatalytic processes.* **Kondratenko, Evgenii V., et al.** 11, 2013, Energy and Environmental Science, Vol. 6, pp. 3112-3135.

10. *Conversion of carbon dioxide into methanol – a potential liquid fuel: Fundamental challenges and opportunities (a review).* **Ganesh, Ibram.** 31, 2014, Renewable & Sustainable Energy Reviews, Vol. 31, pp. 221-257.

11. *The gas-phase destruction of interstellar carbon dioxide: Calculations on the reactions between CO2 and H2 and between CO2 and H.* **Talbi, D. and Herbst, E.** 3, 2002, Astronomy and Astrophysics, Vol. 386, pp. 1139-1142.

12. *Electrochemical reduction of carbon dioxide at various series of copper single crystal electrodes.* **Hori, Y., et al.** 1, 2003, Journal of Molecular Catalysis A-chemical, Vol. 199, pp. 39-47.

13. *Theoretical considerations on the electroreduction of CO to C2 species on Cu(100) electrodes.* **Calle-Vallejo, Federico and Koper, Marc T. M.** 28, 2013, Angewandte Chemie, Vol. 52, pp. 7282-7285.

14. *Reaction Mechanisms for the Electrochemical Reduction of CO2 to CO and Formate on the Cu(100) Surface at 298 K from Quantum Mechanics Free Energy Calculations with Explicit Water.* **Cheng, Tao, Xiao, Hai and Goddard, William A.** 42, 2016, Journal of the American Chemical Society, Vol. 138, pp. 13802-13805.

15. *Structure effects on the energetics of the electrochemical reduction of CO2 by copper surfaces.* **Durand, William J., et al.** 15, 2011, Surface Science, Vol. 605, pp. 1354-1359.

16. *New insights into the electrochemical reduction of carbon dioxide on metallic copper surfaces.* **Kuhl, Kendra P., et al.** 5, 2012, Energy and Environmental Science, Vol. 5, pp. 7050-7059.

17. *Selectivity of CO2 reduction on copper electrodes: The role of the kinetics of elementary steps.* **Nie, Xiaowa, et al.** 9, 2013, Angewandte Chemie, Vol. 52, pp. 2459-2462.

18. *Reaction mechanisms of CO2 electrochemical reduction on Cu(1 1 1) determined with density functional theory.* **Nie, Xiaowa, et al.** 2014, Journal of Catalysis, Vol. 312, pp. 108-122.

19. *How copper catalyzes the electroreduction of carbon dioxide into hydrocarbon fuels.* **Peterson, Andrew, et al.** 9, 2010, Energy and Environmental Science, Vol. 3, pp. 1311-1315.

20. *Spectroscopic Observation of a Hydrogenated CO Dimer Intermediate During CO Reduction on Cu(100) Electrodes.* **Pérez-Gallent, Elena, et al.** 13, 2017, Angewandte Chemie, Vol. 56, pp. 3621-3624.

21. *Atomistic Mechanisms Underlying Selectivities in C1 and C2 Products from Electrochemical Reduction of CO on Cu(111).* **Xiao, Hai, Cheng, Tao és Goddard, William A.** 1, 2017., Journal of the American Chemical Society, 139. kötet, old.: 130-136.

22. *Identification of the Selective Sites for Electrochemical Reduction of CO to C2+ Products on Copper Nanoparticles by Combining Reactive Force Fields, Density Functional Theory, and Machine Learning.* **Huang, Yufeng, et al.** 12, 2018, ACS energy letters, Vol. 3, pp. 2983-2988.

23. *Carbon dioxide conversion into hydrocarbon fuels on defective graphene-supported Cu nanoparticles from first principles.* **Lim, Dong Hee, et al.** 10, 2014, Nanoscale, Vol. 6, pp. 5087-5092.

24. *Optimum Cu nanoparticle catalysts for CO2 hydrogenation towards methanol.* **Zhang, Xue, et al.** 2018, Nano Energy, Vol. 43, pp. 200-209.

25. *The active site of ethanol formation from syngas over Cu4 cluster modified MoS2 catalyst: A theoretical investigation.* **Chen, Jiawang, et al.** 2021, Applied Surface Science, Vol. 540, p. 148301.

26. *Computational studies of electrochemical CO2 reduction on subnanometer transition metal clusters.* **Liu, Cong, et al.** 48, 2014, Physical Chemistry Chemical Physics, Vol. 16, pp. 26584-26599.

27. *Carbon Dioxide Conversion to Methanol over Size-Selected Cu4 Clusters at Low Pressures.* **Liu, Cong, et al.** 27, 2015, Journal of the American Chemical Society, Vol. 137, pp. 8676-8679.

28. *Insight into size dependence of C 2 oxygenate synthesis from syngas on Cu cluster: The effect of cluster size on the selectivity.* **Zhang, Riguang, et al.** 2017, Applied Surface Science, Vol. 407, pp. 282-296.

29. *What Is the Best Size of Subnanometer Copper Clustersfor CO 2 Conversion to Methanol at Cu/TiO 2 Interfaces?A Density Functional Theory Study*. **Tao, Huilin, et al.** 39, 2019, Journal of Physical Chemistry C, Vol. 123, pp. 24118-24132.

30. *Copper Cluster Size Effect in Methanol Synthesis from CO2.* **Yang, Bing, et al.** 19, 2017, Journal of Physical Chemistry C, Vol. 121, pp. 10406-10412.

31. *Dynamic Interplay between Copper Tetramers and IronOxide Boosting CO 2 Conversion to Methanol and Hydrocarbonsunder Mild Conditions.* **Yang, Bing, et al.** 17, 2019, ACS Sustainable Chemistry & Engineering, Vol. 7, pp. 14435-14442.

32. *Catalytic reduction of CO2 by H2 for synthesis of CO, methanol and hydrocarbons: challenges and opportunities.* **Porosoff, Marc D., Yan, Binhang and Chen, Jingguang G.** 1, 2016, Energy and Environmental Science, Vol. 9, pp. 62-73.

33. *Reaction mechanisms of catalytic photochemical CO2 reduction using Re(I) and Ru(II) complexes.* **Kuramochi, Yusuke, Ishitani, Osamu and Ishida, Hitoshi.** 2018, Coordination Chemistry Reviews, Vol. 373, pp. 333-356.

34. *Catalysts and Reaction Pathways for the Electrochemical Reduction of Carbon Dioxide*. **Kortlever, Ruud, et al.** 20, 2015, Journal of Physical Chemistry Letters, Vol. 6, pp. 4073-4082.

35. *Single atom electrocatalysts supported on graphene or graphene-like carbons.* **Fei, Huilong, et al.** 20, 2019, Chemical Society Reviews, Vol. 48, pp. 5207-5241.

36. *A roadmap for graphene.* **Novoselov, K. S., et al.** 7419, 2012, Nature, Vol. 490, pp. 192-200.

37. *Binding of Pt Nanoclusters to Point Defects in Graphene: Adsorption, Morphology, and Electronic Structure.* **Fampiou, Ioanna and Ramasubramaniam, Ashwin.** 11, 2012, Journal of Physical Chemistry C, Vol. 116, pp. 6543-6555.

38. *First-principles study of small Pd–Au alloy clusters on graphene.* **Ji, Wei-xiao, et al.** 99, 2014, RSC Advances, Vol. 4, pp. 55781-55789.

39. *Boron-doped graphene as electrocatalytic support for iridium oxide for oxygen evolution reaction.* **Joshi, Prerna, et al.** 19, 2020, Catalysis Science & Technology, Vol. 10, pp. 6599-6610.

40. *DFT studies of Ni cluster on graphene surface: effect of CO2 activation.* **Xu, He, et al.** 99, 2016, RSC Advances, Vol. 6, pp. 96545-96553.

41. *Will Any Crap We Put into Graphene Increase Its Electrocatalytic Effect.* **Wang, Lu, Sofer, Zdenek and Pumera, Martin.** 1, 2020, ACS Nano, Vol. 14, pp. 21-25.

42. *Highly selective electrocatalytic CO 2 reduction to ethanol by metallic clusters dynamically formed from atomically dispersed copper.* **Xu, Haiping, et al.** 8, 2020, Nature Energy, Vol. 5, pp. 623-632.

43. *Architectural Design for Enhanced C2 Product Selectivity in Electrochemical CO2 Reduction Using Cu-Based Catalysts: A Review.* **Xiao, Changlong and Zhang, Jie.** 5, 2021, ACS Nano, Vol. 15, pp. 7975-8000.

44. *Generalized Gradient Approximation Made Simple.* **Perdew, John P., Burke, Kieron és Ernzerhof, Matthias.** 18, 1996., Physical Review Letters, 77. kötet, old.: 3865-3868.

45. *Semiempirical GGA-type density functional constructed with a long-range dispersion correction.* **Grimme, Stefan.** 15, 2006., Journal of Computational Chemistry, 27. kötet, old.: 1787-1799.

46. *Energy-adjustedab initio pseudopotentials for the second and third row transition elements.* **Andrae, D., és mtsai.** 2, 1990., Theoretical Chemistry Accounts, 77. kötet, old.: 123-141.

47. *Universal solvation model based on solute electron density and on a continuum model of the solvent defined by the bulk dielectric constant and atomic surface tensions.* **Marenich, Aleksandr V., Cramer, Christopher J. és Truhlar, Donald G.** 18, 2009., Journal of Physical Chemistry B, 113. kötet, old.: 6378-6396.

48. *Can a single valence electron alter the electrocatalytic activity and selectivity for CO2 reduction on the subnanometer scale.* **Raju, Rajesh Kumar, Rodriguez, Paramaconi and Johnston, Roy L.** 23, 2019, Journal of Physical Chemistry C, Vol. 123, pp. 14591-14609.

49. *Reaction mechanism and kinetics for CO 2 reduction on nickel single atom catalysts from quantum mechanics.* **Hossain, Delowar, et al.** 1, 2020, Nature Communications, Vol. 11, p. 2256.

50. *Unravelling the origin of intermolecular interactions using absolutely localized molecular orbitals.* **Khaliullin, Rustam Z, et al.** 36, 2007, Journal of Physical Chemistry A, Vol. 111, pp. 8753-8765.

51. *Intermolecular interactions from a natural bond orbital, donor-acceptor viewpoint.* **Reed, Alan E., Curtiss, Larry A. and Weinhold, Frank.** 6, 1988, Chemical Reviews, Vol. 88, pp. 899-926.

52. *Nucleus-independent chemical shifts (NICS) as an aromaticity criterion.* **Chen, Zhongfang, et al.** 10, 2005, Chemical Reviews, Vol. 105, pp. 3842-3888.

53. *Metals on Graphene: Interactions, Growth Morphology, and Thermal Stability.* **Liu, Xiaojie, et al.** 1, 2013, Crystals, Vol. 3, pp. 79-111.

54. *Trends in the Adsorption of 3d Transition Metal Atoms onto Graphene and Nanotube Surfaces: A DFT Study and Molecular Orbital Analysis.* **Valencia, Hubert, Gil, Adrià and Frapper, Gilles.** 33, 2010, Journal of Physical Chemistry C, Vol. 114, pp. 14141-14153.

55. *Combinatorial Search for High-Activity Hydrogen Catalysts Based on Transition-Metal-Embedded Graphitic Carbons.* **Choi, Woon Ih, et al.** 23, 2015, Advanced Energy Materials, Vol. 5, p. 1501423.

56. *Boron-Doped Graphene: Scalable and Tunable p-Type Carrier Concentration Doping.* **Wang, Lu, et al.** 44, 2013, Journal of Physical Chemistry C, Vol. 117, pp. 23251-23257.

57. *Author Correction: Dopant-induced electron localization drives CO2 reduction to C2 hydrocarbons.* **Zhou, Yansong, és mtsai.** 12, 2019., Nature Chemistry, 11. kötet, old.: 1167-1167.

58. *Nonconventional C–H···Cu Interaction Between Copper Cun Clusters (n = 3–20) and Aromatic Compounds.* **Rangel-Peña, Uriel J., et al.** 2020, Journal of Cluster Science, pp. 1-19.

59. *Phenomenological Shell Model and Aromaticity in Metal Clusters.* **Holtzl, T, et al.** 2010.

60. *Full atomistic reaction mechanism with kinetics for CO reduction on Cu(100) from ab initio molecular dynamics free-energy calculations at 298 K.* **Cheng, Tao, Xiao, Hai and Goddard, William A.** 8, 2017, Proceedings of the National Academy of Sciences of the United States of America, Vol. 114, pp. 1795-1800.

61. *The oxygen reduction reaction mechanism on Pt(111) from density functional theory calculations.* **Tripkovic, Vladimir, et al.** 27, 2010, Electrochimica Acta, Vol. 55, pp. 7975-7981.

62. *First-Principles Analysis of the Initial Electroreduction Steps of Oxygen over Pt(111).* **Janik, Michael J., Taylor, Christopher D. and Neurock, Matthew.** 1, 2009, Journal of The Electrochemical Society, Vol. 156.